From Analog Signals to Digital Information

Alex Kopaigorodski and Moshe Porat
Department of Electrical Engineering
Technion, Haifa, Israel
alexkop@tx.technion.ac.il, mp@ee.technion.ac.il

ABSTRACT

Many information-processing applications are based on digital data although the origin of most sources of information is analog. A new signal sampling and representation framework for such purposes is introduced in this work. We use prolate spheroidal wave functions (PSWF) to represent analog signals by digital information. The proposed method can be applied to reconstruct signals on a finite interval from a finite number of discrete samples. It is shown that, contrary to the Nyquist approximation, the reconstruction error of the proposed technique can be made as small as desired. The new method is applicable to general signals including two-dimensional sources of images. Experimental results are presented and discussed. Our conclusion is that the proposed approach to signal representation using PSWF could be superior to presently available methods and may be instrumental in most practical cases of digital signals, which are naturally of finite support.

KEYWORDS

Analog to Digital Conversion, Sampling Theorem, Approximation, Reconstruction, Prolate Spheroidal Wave Functions.

1 INTRODUCTION

Nyquist sampling theorem is widely accepted as a means of representing band-limited signals by their digital samples. Its main drawbacks, however, are that practical signals are time-limited and therefore not band-limited and that in order to reconstruct a band-limited signal an infinite number of samples are required. Nevertheless, although in most cases Nyquist theorem cannot be used to perfectly reconstruct signals, it can be used as a reasonable approximation for the acquisition of most signals.

In this work, we propose a new approach to the digitization task, providing a better approximation than uniform Nyquist-based sampling. The proposed method is more complex than uniform sampling, however, suitable hardware can easily cope with the added complexity. On the other hand, in order to get the same approximation error, the proposed method will require significantly fewer samples than uniform sampling.

According to the sampling theorem, a band-limited signal $f(x)$ can be represented as a function of its discrete samples $f(n/2\omega)$. Mathematically, the signal representation is as follows:

$$f(x) = \sum_{n=-\infty}^{\infty} f\left(\frac{n}{2\omega}\right) \frac{\sin\left(2\pi\omega\left(\mathrm{x} - \frac{\mathrm{n}}{2\omega}\right)\right)}{2\pi\omega\left(\mathrm{x} - \frac{\mathrm{n}}{2\omega}\right)}. \qquad (1)$$

It is evident that the signal reconstruction is affected by all its samples. Due to the scaling property of the Fourier transform, without loss of generality we will set the interval to be $[-1,1]$ in this paper and only the bandwidth will be changed.

Figure 1 depicts a band-limited signal and its *finite* sum approximation according to:

$$f(x) = \sum_{n=-N}^{N} f\left(\frac{n}{2\omega}\right) \frac{\sin\left(2\pi\omega\left(x - \frac{n}{2\omega}\right)\right)}{2\pi\omega\left(x - \frac{n}{2\omega}\right)}, \quad N = \lfloor 2\omega \rfloor. \tag{2}$$

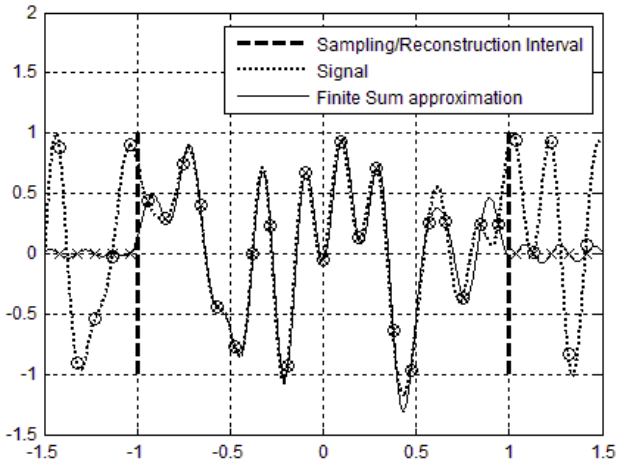

Figure 1. Signal reconstruction using a finite number of samples within a given interval. As can be seen, an error is likely to occur mainly near both ends of the interval.

Due to the decay rate of the *Sinc* function, it is reasonable to assume that adjacent samples affect the result more than samples that are far from the reconstruction point, in a reciprocal manner to the distance. It can be seen in Figure 1 that at the edges of the interval the approximation error is larger than in the middle of the interval. This could be significant for short time support signals.

Generally, the error is signal dependent. But the average error can be analyzed using a stochastic band-limited signal model:

$$f(x) = \sum_{n=-M}^{M} c_n \frac{sin\left(2\pi\omega\left(x - \frac{n}{2\omega}\right)\right)}{2\pi\omega\left(x - \frac{n}{2\omega}\right)}, \quad M \gg \lfloor 2\omega \rfloor \tag{3}$$

where c_n are zero-mean IID random variables. In this model the signals have a flat spectrum.

Assuming that only $2N+1$ samples in an interval $[-1,1]$ are known, Equation (3) can be approximated by:

$$\hat{s}(x) = \sum_{n=-N}^{N} c_n \frac{sin\left(2\pi\omega\left(x - \frac{n}{2\omega}\right)\right)}{2\pi\omega\left(x - \frac{n}{2\omega}\right)}, \quad N = \lfloor 2\omega \rfloor \tag{4}$$

and the approximation error is then given by:

$$E\left\{\|\hat{s}(x) - s(x)\|_{L_2}^2\right\} = E\left\{\int_{-1}^{1} |\hat{s}(x) - s(x)|^2 dx\right\} = \sigma_c^2 \sum_{M \geq |n| > N} P(n), \tag{5}$$

which is proportional to:

$$P(n) = \int_{-1}^{1} \left| \frac{sin\left(2\pi\omega\left(x - \frac{n}{2\omega}\right)\right)}{2\pi\omega\left(x - \frac{n}{2\omega}\right)} \right|^2 dx. \tag{6}$$

Figure 2 depicts numerical calculation of (5). It is apparent that the approximation error is decreasing with the bandwidth.

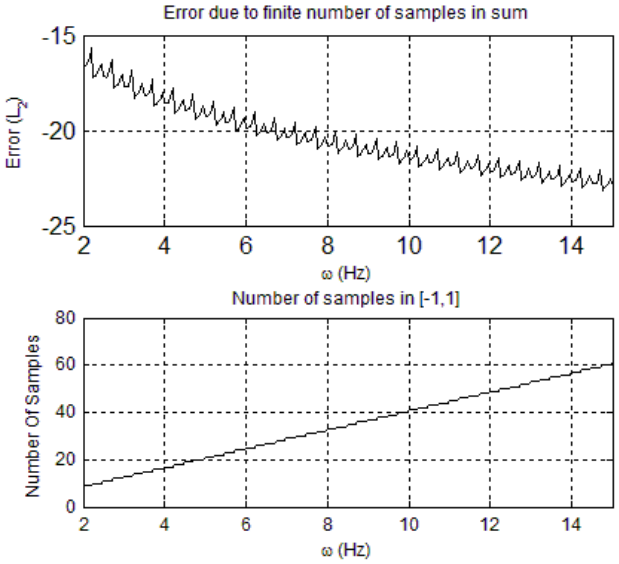

Figure 2. Approximation error and SNR. The horizontal axis indicates the bandwidth of the signal.

This result is due to the fact that fewer samples are adjacent to edges and thus the approximation error is smaller.

ISBN: 978-1-941968-14-7 ©2015 SDIWC

2 THE PROPOSED APPROACH

Given a band-limited signal $y(t)$, the goal is to find an N-dimensional signal $\tilde{y}(t)$ minimizing $\|y(t) - \tilde{y}(t)\|_{L_2[-1,1]}$. Generally, nor $y(t)$ and neither $\tilde{y}(t)$ vanish outside $[-1,1]$. It is also possible that $\|y(t) - \tilde{y}(t)\|_{L_2[-1,1]}$ is large.

The proposed approximation is based on Prolate Spheroidal Wave Functions (PSWF) of order zero. Although PWSF were studied exhaustively in the past, there is little research akin to sampling and reconstruction using PSWF. In [1] the authors proposed to use PWSF to extrapolate a signal known in $[-1,1]$. In [2] the author proposed to interpolate band-limited functions using PSWF, however, did not present a concrete reconstruction scheme though he did state that PWSF are mathematically intractable and presented asymptotic expansion.

Our approximation is based on three prominent properties of PSWF: *(i)* Prolate Spheroidal Wave Functions of order zero comprise an orthonormal basis in $L_2[-1,1]$. *(ii)* The PSWF are bounded. According to [3] Equations (58) and (60) there is $N > 0$, such that for all $n > N$ the following holds:

$$\psi_n^{\omega}(x) \le \sqrt{n + 0.5}\,. \tag{7}$$

(iii) The eigenvalues of PWSF have a distinctive pattern:

$$\begin{array}{cc} \omega|\lambda_n^{\omega}|^2 \approx 1 & n \le 4\omega \\ 0 < \omega|\lambda_n^{\omega}|^2 < 1 & 4\omega < n \le 4\omega + 6 \\ \omega|\lambda_n^{\omega}|^2 \approx 0 & 4\omega + 6 < n\,. \end{array} \tag{8}$$

It can also be shown that the eigenvalues $\{\lambda_n^{\omega}\}_{n=0}^{\infty}$ have very fast decay [4]. Approximately the first $\lfloor 4\omega \rfloor$ values of $\omega|\lambda_n^{\omega}|^2$ are very close to 1. Then only a small number of eigenvalues are between 0 and 1, while the rest are very close to zero. Figure 3 depicts a few distributions of PSWF eigenvalues.

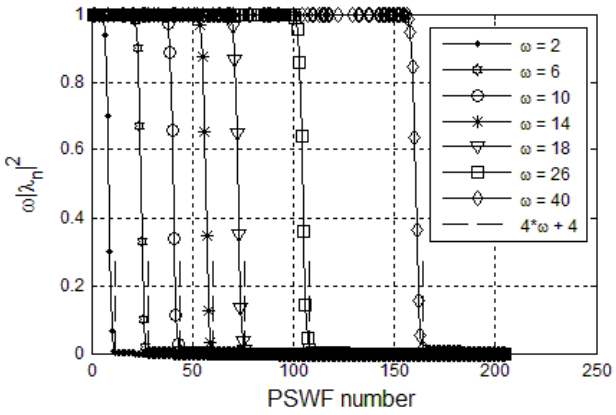

Figure 3. The distribution of PSWF eigenvalues, as a function of the bandwidth ω.

As a result, it will be shown that the approximation error of using PSWF to represent a signal can be made small due to the fast eigenvalue decay. In fact, for $n \ge 4\omega + 6$ the eigenvalues λ_n^{ω} have a more than exponential decay. An asymptotic bound is found in numerous numerical calculations:

$$\begin{array}{c} |\lambda_n^{\omega}| \le |\lambda_m^{\omega}| \cdot e^{-\eta(n-m)}, \\ n \ge m \ge \lceil 4\omega + 6 \rceil\,. \end{array} \tag{9}$$

Figure 4 depicts several numerical calculations.

It is straightforward to show that the eigenfunctions $\{\Psi_n(u)\}_{n=0}^{\infty}$ constitute an orthonormal basis for $L_2[-\omega, \omega]$. Hence it is possible to represent a signal in the frequency domain as a linear combination of the basis functions:

$$\Psi_n(u) = \begin{cases} \frac{1}{\sqrt{\omega}} \psi_n^{\omega}\left(\frac{u}{\omega}\right) & -\omega \le u \le \omega \\ 0 & |u| > \omega \end{cases}, \tag{10}$$

such that:

$$\left\| Y(\xi) - \sum_{n=0}^{N-1} a_n \cdot \Psi_n(u) \right\|_{L_2[-\omega,\omega]} \xrightarrow{N\to\infty} 0\,, \tag{11}$$

$$a_n = \langle Y(\xi), \Psi_n(\xi) \rangle_{L_2[-\omega,\omega]}\,, \tag{12}$$

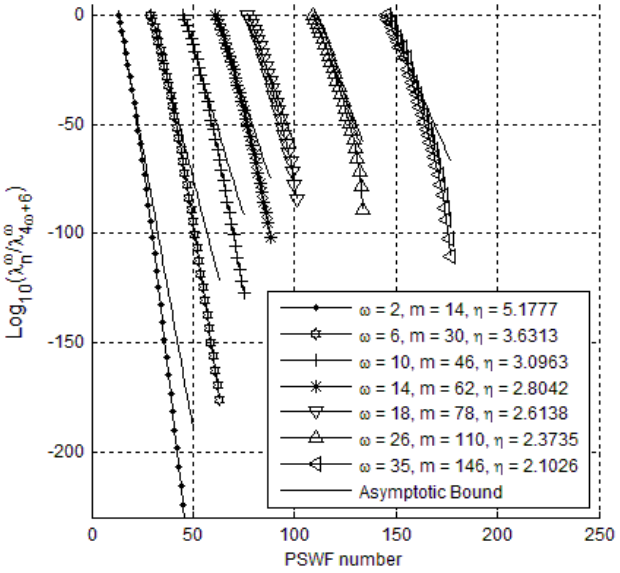

Figure 4. Numerical presentation of the PSWF eigenvalue decay.

where $Y(\xi)$ is the Fourier transform of $y(x)$ and $\{a_n\}_{n=0}^{\infty}$ are the representation coefficients. By using Parseval's identity, it is possible to get the following set of equations (Appendix A):

$$\left\| y(x) - \sum_{n=0}^{N-1} a_n \cdot \lambda_n \sqrt{\omega} \cdot \psi_n(x) \right\|_{L_2[-\infty,\infty]} \xrightarrow{N\to\infty} 0, \quad (13)$$

$$\left\| y(x) - \sum_{n=0}^{N-1} a_n \cdot \lambda_n \sqrt{\omega} \cdot \psi_n(x) \right\|_{L_2[-1,1]} \leq \sqrt{\omega \sum_{n=N}^{\infty} |a_n \cdot \lambda_n|^2}\,, \quad (14)$$

$$\sqrt{\sqrt{\omega} \sum_{n=N}^{\infty} |a_n \cdot \lambda_n|^2} \leq \sqrt{\omega} \cdot \sup_{n\geq N} |a_n| \cdot \sqrt{\sum_{n=N}^{\infty} |\lambda_n|^2}\,, \quad (15)$$

which indicate the norm of the error.

The PSWF expansion is stable in the sense that a small change in the coefficients $\{a_n\}_{n=0}^{\infty}$ causes only a small change in the approximation error:

$$\left\| y(x) - \sum_{n=0}^{N-1} (a_n + \Delta a_n) \cdot \lambda_n \sqrt{\omega} \cdot \psi_n(x) \right\|_{L_2[-1,1]} \leq \sqrt{\sqrt{\omega} \sum_{n=N}^{\infty} |a_n \cdot \lambda_n|^2} + \sqrt{\sum_{n=0}^{N-1} |\Delta a_n|^2}\,. \quad (16)$$

Furthermore, as known from Fourier Theory, L_2 convergence does not necessarily imply pointwise and uniform convergence. Here, however, in the PSWF reconstruction, L_2 convergence does imply uniform convergence and there is no Gibbs-like phenomenon. In fact, it can be shown that for $x \in [-1,1]$ we get (Appendix A):

$$\left| y(x) - \sqrt{\omega} \sum_{n=0}^{N-1} a_n \cdot \lambda_n \cdot \psi_n(x) \right| \leq \sqrt{\omega} \left| \sum_{n=N}^{\infty} \lambda_n a_n \cdot \psi_n(x) \right|, \quad (17)$$

which means that the error can be made as small as desired independently of the represented signal.

Our analysis shows that most band-limited signals can be reconstructed by approximately the $\lceil 4\omega + 6 \rceil$ first eigenfunctions of PSWF. According to (18), $\omega|\lambda_n|^2$ is the ratio between the PSWF energy in $[-1,1]$ to the PSWF total energy. From (8), approximately the $\lceil 4\omega + 6 \rceil$ first eigenfunctions have significant energy inside $[-1,1]$ while other eigenfunctions have most of their energy outside $[-1,1]$. As a result, only the $\lceil 4\omega + 6 \rceil$ first eigenfunctions play a role in band-limited signal approximation inside $[-1,1]$:

$$\omega|\lambda_n|^2 = \frac{\|\psi_n(x)\|^2_{L_2[-1,1]}}{\|\psi_n(x)\|^2_{L_2[-\infty,\infty]}}. \quad (18)$$

It is possible to perform numerical integration in order to calculate the expansion coefficients $\{a_n\}_{n=0}^{\infty}$. An apparent drawback of numerical integration is the requirement for many samples of the signal and thus greater complexity. It is thus proposed to use an alternative approach that utilizes the PSWF properties. The sampling is not uniform, and in addition it requires a matrix for vector multiplication. The expansion coefficients are calculated using:

$$\tilde{\underline{a}} = \underline{\underline{\Psi}}^{-1}(\underline{x})y(\underline{x}), \tag{19}$$

where:

$$\underline{\underline{\Psi}}(\underline{x}) = \begin{bmatrix} \psi_0(x_0) & \cdots & \psi_{N-1}(x_0) \\ \vdots & \ddots & \vdots \\ \psi_0(x_{N-1}) & \cdots & \psi_{N-1}(x_{N-1}) \end{bmatrix}, \tag{20}$$

After mathematical derivations we get (see Appendix A):

$$\left\|\tilde{\underline{a}} - \underline{a}\right\|_{l_2} \le \left\|\underline{\underline{\Psi}}(\underline{x})^{-1}\right\|_{l_2} \sqrt{N\omega} \left| \sum_{n=N}^{\infty} \lambda_n a_n \cdot \sqrt{n+0.5} \right|, \tag{21}$$

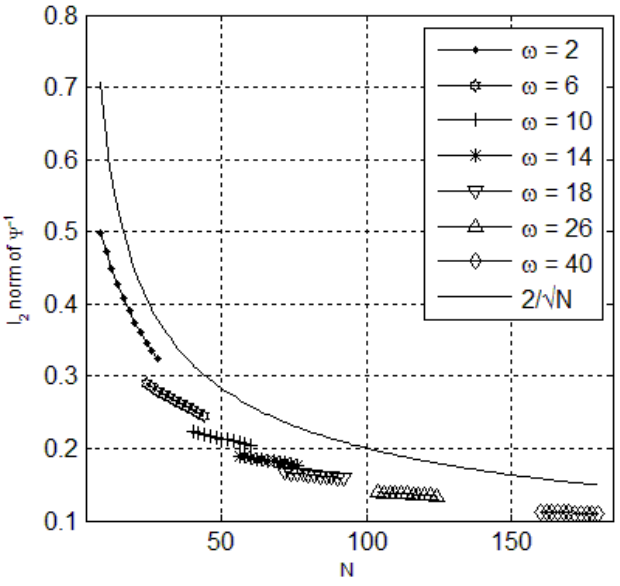

Figure 5. $\boldsymbol{\Psi(\underline{x}_{Zeros})^{-1}}$ norm bound. As can be seen, all the values are below the $\frac{2}{\sqrt{N}}$ curve.

and

$$\underline{a} = \left[\sqrt{\omega}\lambda_0 a_0, \ldots, \sqrt{\omega}\lambda_{N-1} a_{N-1}\right]^T. \tag{22}$$

From (21) it can be deduced that the coefficients error is proportional to $\left\|\underline{\underline{\Psi}}(\underline{x}_{Zeros})^{-1}\right\|_{l_2}$. Through numerical analysis it can be shown that the following holds:

$$\left\|\underline{\underline{\Psi}}(\underline{x}_{Zeros})^{-1}\right\|_{l_2} \le \frac{2}{\sqrt{N}}. \tag{23}$$

Figure 5 depicts numerical calculations of (23). As a result, we can show that (see Appendix A):

$$\left\|\tilde{\underline{a}} - \underline{a}\right\|_{l_2} \le 2\sqrt{\omega} \left| \sum_{n=N}^{\infty} \lambda_n a_n \cdot \sqrt{n+0.5} \right|. \tag{24}$$

The reconstruction error of a band-limited signal has two parts. The first part is due to the finite expansion (14). The second part is due to the expansion coefficient calculation (19). Combining (14), (16) and (24) yields:

$$\left\| y(x) - \sum_{n=0}^{N-1} \tilde{a}_n \cdot \psi_n(x) \right\|_{L_2[-1,1]} \le \sqrt{\omega \sum_{n=N}^{\infty} |a_n \cdot \lambda_n|^2 + 2\sqrt{\omega} \left| \sum_{n=N}^{\infty} \lambda_n a_n \cdot \sqrt{n+0.5} \right|}. \tag{25}$$

Using (9) to evaluate the right hand side of (25) we get:

$$\sqrt{\sum_{n=N}^{\infty} |a_n \cdot \lambda_n^{\omega}|^2} \le \sup_{n \ge N} |a_n| \cdot \frac{|\lambda_N^{\omega}|}{\sqrt{1 - e^{-2\eta}}}, \tag{26}$$

$$\left| \sum_{n=N}^{\infty} \lambda_n^{\omega} a_n \cdot \sqrt{n+0.5} \right| \le \sqrt{\sum_{n=N}^{\infty} |a_n|^2 \cdot |\lambda_N^{\omega}|} \frac{\sqrt{N+1}}{(1 - e^{-2\eta})}, \tag{27}$$

$$\sup_{n\geq N}|a_n| \leq \sqrt{\sum_{n=N}^{\infty}|a_n|^2} \leq \|y\|_{L_2}\,. \qquad (28)$$

Finally, it can be shown that (25) is bounded by:

$$\sqrt{\omega}\sqrt{\sum_{n=N}^{\infty}|a_n|^2}\cdot|\lambda_N^{\omega}|\cdot\left(\frac{1}{\sqrt{1-e^{-2\eta}}}+\frac{2\sqrt{N+1}}{(1-e^{-2\eta})}\right). \qquad (29)$$

The reconstruction error bound is a product of three factors. The first factor is the residue of the signal's series expansion, therefore bounded by the signal's energy (28). The second factor is the PSWF eigenvalue of order N. The third factor is proportional to $\sqrt{N+1}$. According to (9), the PSWF eigenvalues have more than exponential decay. Consequently, (29) is dominated by the PSWF eigenvalue of order N, and as such has more than exponential decay.

Figure 6 depicts numerical calculation of the reconstruction error bound without a signal dependent factor:

$$\sqrt{\omega}\cdot|\lambda_N^{\omega}|\cdot\left(\frac{1}{\sqrt{1-e^{-2\eta}}}+\frac{2\sqrt{N+1}}{(1-e^{-2\eta})}\right). \qquad (30)$$

It is evident that contrary to the sampling theorem, an additional sampling point results in significant improvement of the reconstruction error. In numerical experiments it is observed that the reconstruction error bound is not tight and in the vast majority of cases $\lceil 4\omega\rceil + 4$ samples will yield good reconstructions.

3 RESULTS

In order to compare the two methods for the same number of samples, Monte-Carlo simulations [5] were carried out in this work. As can be seen in Figure 7, changing the number of samples for example from $\lceil 4\omega\rceil + 4$ to $\lceil 4\omega\rceil + 6$ hardly improves the approximation error for the uniform method, while affecting the new proposed approach significantly, by approximately $20dB$. A related two-dimensional result is shown in Fig. 8.

4 CONCLUSION

A new framework for digital signal representation has been introduced in this work. We have compared it with the standard bandlimited interpolation and with a fast decaying kernel. The main advantage of the new method over uniform sampling is that here a small increase in oversampling results in a significant decrease of the approximation error. This behavior of the approximation error is due to the fast decay of the eigenvalues of the PSWF- λ_N^{ω} for $n \geq \lceil 4\omega\rceil + 6$.

Our conclusion is that the proposed approach is superior to presently available methods. The new method could be instrumental in most practical cases of processing of finite support signals [6],[7], especially in cases where the sampling-interval multiplied by the bandwidth is small.

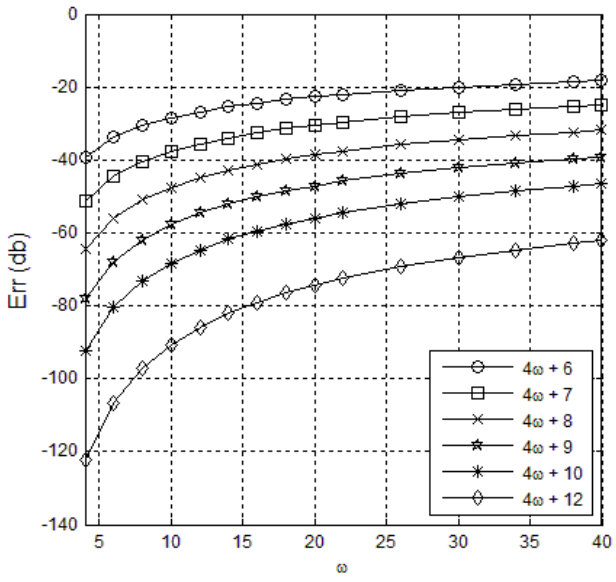

Figure 6. Reconstruction Error Bound as a function of the bandwidth for various numbers of sampling points.

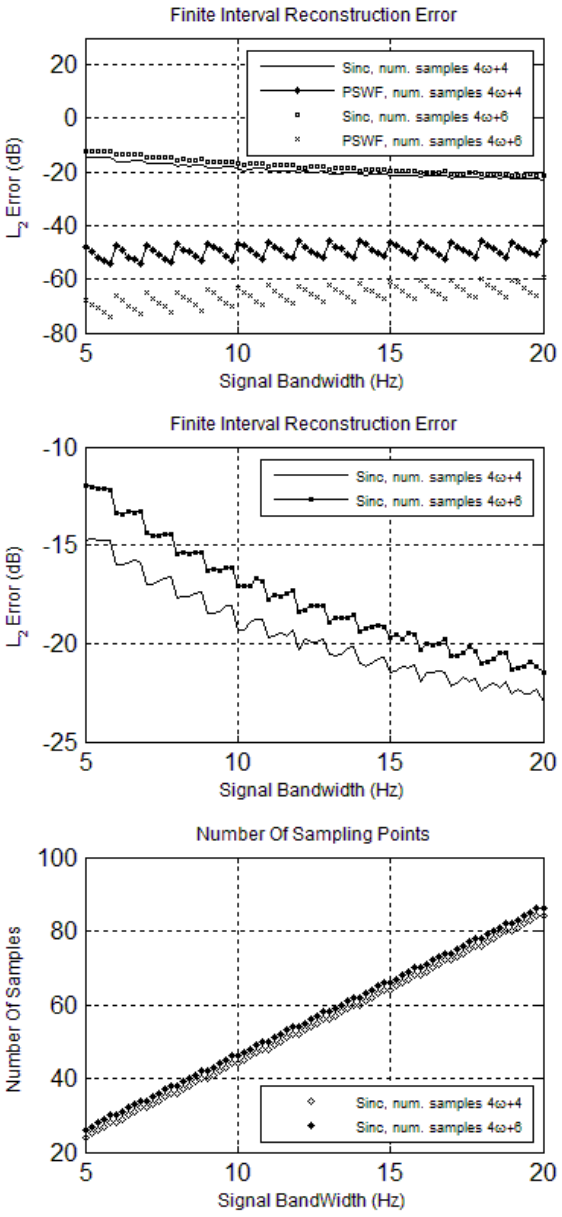

Figure 7. Approximation error comparison. Shown are the SNR (top) and the number of sample (bottom) as a function of the signal bandwidth.

APPENDIX A

Derivation of (13):

$$\mathcal{F}^{-1}\{\Psi_n(\xi)\} \underset{Def.}{=} \int_{-\infty}^{\infty} \Psi_n(\xi) e^{j2\pi x\xi} d\xi \underset{definition}{=} \int_{-\omega}^{\omega} \frac{1}{\sqrt{\omega}} \psi_n^{\omega}\left(\frac{\xi}{\omega}\right) e^{j2\pi x\xi} d\xi \underset{\substack{Variable \\ Change}}{=}$$

$$\sqrt{\omega} \int_{-1}^{1} \psi_n^{\omega}(u) e^{j2\pi\omega xu} du \underset{definition}{=} \lambda_n \sqrt{\omega} \cdot \psi_n^{\omega}(x).$$

$$\left\| Y(\xi) - \sum_{n=0}^{N-1} a_n \cdot \Psi_n(u) \right\|_{L_2[-\omega,\omega]} \underset{definition}{=}$$

Figure 8. The effect of the new approach on images. As can be seen, in short finite-support signals (vertical segments marked at the 2nd image from the left) the edges of the segments are distorted when uniform sampling is used (white vertical lines in the 3rd image from the left) while the proposed method provides superior continuous reconstruction (4th image).

$$\left\| Y(\xi) - \sum_{n=0}^{N-1} a_n \cdot \Psi_n(u) \right\|_{L_2[-\infty,\infty]}$$

$$\underset{\substack{Parseval's \\ Identity}}{=} \left\| y(x) - \sum_{n=0}^{N-1} a_n \cdot \mathcal{F}^{-1}\{\Psi_n(\xi)\} \right\|_{L_2[-\infty,\infty]} \underset{\substack{Eq. \\ Above}}{=}$$

$$\left\| y(x) - \sum_{n=0}^{N-1} a_n \cdot \lambda_n \sqrt{\omega} \cdot \psi_n^{\omega}(x) \right\|_{L_2[-\infty,\infty]}$$

Derivation of (14):

$$\left\| y(x) - \sum_{n=0}^{N-1} a_n \cdot \lambda_n \sqrt{\omega} \cdot \psi_n(x) \right\|_{L_2[-1,1]} \underset{Triangle\ inequality}{\leq}$$

$$\left\| y(x) - \sum_{n=0}^{M} a_n \cdot \lambda_n \sqrt{\omega} \cdot \psi_n(x) \right\|_{L_2[-1,1]}$$

$$+ \left\| \sum_{n=N}^{M} a_n \cdot \lambda_n \sqrt{\omega} \cdot \psi_n(x) \right\|_{L_2[-1,1]} \underset{Intg}{\leq}$$

$$\left\| y(x) - \sum_{n=0}^{M} a_n \cdot \lambda_n \sqrt{\omega} \cdot \psi_n(x) \right\|_{L_2[-\infty,\infty]} + \sqrt{\omega \sum_{n=N}^{M} |\lambda_n a_n|^2}_{L_2[-1,1]}$$

By taking $M \to \infty$ and the orthogonality of $\{\psi_n\}_{n=0}^{\infty}$ one can get the result.

Derivation of (17):

$$\left| y(x) - \sqrt{\omega} \sum_{n=0}^{N-1} a_n \cdot \lambda_n \cdot \psi_n(x) \right| \underset{Triangle\ inequality}{\leq}$$

$$\left| y(x) - \sqrt{\omega} \sum_{n=0}^{M-1} a_n \cdot \lambda_n \cdot \psi_n(x) \right|$$

$$+ \sqrt{\omega} \left| \sum_{n=N}^{M-1} a_n \cdot \lambda_n \cdot \psi_n(x) \right|$$

$$\left| y(x_0) - \sqrt{\omega} \sum_{n=0}^{M-1} a_n \cdot \lambda_n \cdot \psi_n(x_0) \right| \underset{FT}{=}$$

$$\left|\int_{-\omega}^{\omega}\left(Y(\xi)-\sum_{n=0}^{M-1}a_n\Psi_n(\xi)\right)e^{j2\pi x_0\xi}d\xi\right| \leq$$
$$\int_{-\omega}^{\omega}\left|Y(\xi)-\sum_{n=0}^{M-1}a_n\Psi_n(\xi)\right|d\xi \underset{\substack{Cauchy-Schwarz\\ inequality}}{\leq}$$
$$2\omega\sqrt{\int_{-\omega}^{\omega}\left|Y(\xi)-\sum_{n=0}^{M-1}a_n\Psi_n(\xi)\right|^2 d\xi} \xrightarrow{M\to\infty} 0$$

Therefore:

$$\left|y(x_0)-\sqrt{\omega}\sum_{n=0}^{N-1}a_n\cdot\lambda_n\cdot\psi_n(x_0)\right| \leq \sqrt{\omega}\left|\sum_{n=N}^{\infty}a_n\cdot\lambda_n\cdot\psi_n(x_0)\right|$$

Derivation of (21) and (24):

$$\left\|\tilde{\underline{a}}-\underline{a}\right\|_{l_2} = \left\|\Psi(\underline{x})^{-1}y(\underline{x})-\underline{a}\right\|_{l_2} =$$
$$\left\|\Psi(\underline{x})^{-1}(y(\underline{x})-\Psi(\underline{x})\underline{a})\right\|_{l_2} \underset{\substack{matrix\\ norm}}{\leq}$$
$$\left\|\Psi(\underline{x})^{-1}\right\|_{l_2}\left\|y(\underline{x})-\Psi(\underline{x})\underline{a}\right\|_{l_2}$$

$$\left\|y(\underline{x})-\Psi(\underline{x})\underline{a}\right\|_{l_2}^2 = \sum_{m=0}^{N-1}\left|y(x_m)-\sqrt{\omega}\sum_{n=0}^{N-1}\lambda_n a_n\psi_n(x_m)\right|^2 \underset{17}{\leq}$$
$$\sum_{m=0}^{N-1}\left|\sum_{n=N}^{\infty}\sqrt{\omega}\lambda_n a_n\cdot\psi_n(x_m)\right|^2 \underset{7}{\leq} \sum_{m=0}^{N-1}\left|\sum_{n=N}^{\infty}\sqrt{\omega}\lambda_n a_n\cdot\sqrt{n+0.5}\right|^2$$
$$= N\omega\left|\sum_{n=N}^{\infty}\lambda_n a_n\cdot\sqrt{n+0.5}\right|^2$$

From (23) stems:

$$\left\|\tilde{\underline{a}}-\underline{a}\right\|_{l_2} \leq 2\sqrt{\omega}\left|\sum_{n=N}^{\infty}\lambda_n a_n\cdot\sqrt{n+0.5}\right|.$$

Derivation of (26):

$$\sqrt{\sum_{n=N}^{\infty}|\lambda_n^{\omega}|^2} \leq \lambda_m^{\omega}\cdot\sqrt{\sum_{n=N}^{\infty}|e^{-\eta(n-m)}|^2} = \lambda_m^{\omega}\cdot e^{\eta m}\sqrt{\sum_{n=N}^{\infty}e^{-2\eta n}} =$$
$$\lambda_m^{\omega}\cdot e^{\eta m}\sqrt{\frac{1}{1-e^{-2\eta}}-\frac{1-e^{-2\eta N}}{1-e^{-2\eta}}} = \lambda_m^{\omega}\cdot e^{\eta m}\sqrt{\frac{e^{-2\eta N}}{1-e^{-2\eta}}}$$
$$= \lambda_m^{\omega}\cdot\frac{e^{-\eta(N-m)}}{\sqrt{1-e^{-2\eta}}}.$$

By choosing $m = N$:

$$\sqrt{\sum_{n=N}^{\infty}|\lambda_n^{\omega}|^2} \leq \frac{\lambda_N^{\omega}}{\sqrt{1-e^{-2\eta}}},$$

Therefore:

$$\sqrt{\sum_{n=N}^{\infty}|a_n\cdot\lambda_n^{\omega}|^2} \leq \sup_{n\geq N}|a_n|\sqrt{\sum_{n=N}^{\infty}|\lambda_n^{\omega}|^2} \leq \sup_{n\geq N}|a_n|\cdot\frac{|\lambda_N^{\omega}|}{\sqrt{1-e^{-2\eta}}}.$$

Derivation of (27):

$$\left|\sum_{n=N}^{\infty}\lambda_n^{\omega}a_n\cdot\sqrt{n+0.5}\right| \underset{\substack{Cauchy-Schwarz\\ inequality}}{\leq} \sqrt{\sum_{n=N}^{\infty}|a_n|^2}\sqrt{\sum_{n=N+1}^{\infty}|\lambda_{n-1}^{\omega}|^2 n}$$

$$\sqrt{\sum_{n=N+1}^{\infty}|\lambda_{n-1}^{\omega}|^2 n} \leq \lambda_m^{\omega}\cdot\sqrt{\sum_{n=N+1}^{\infty}n|e^{-\eta(n-1-m)}|^2} =$$

$$\lambda_m^{\omega}\cdot e^{\eta(m+1)}\sqrt{\sum_{n=N+1}^{\infty}ne^{-2\eta n}}$$

$$\sum_{n=0}^{N-1}n\cdot e^{-an} = \frac{e^{-a}-e^{-aN}(e^{-a}+N-Ne^{-a})}{(1-e^{-a})^2},$$

$$\sum_{n=N+1}^{\infty}ne^{-2a\cdot n} = \sum_{n=0}^{\infty}ne^{-2a\cdot n}-\sum_{n=0}^{N}ne^{-2a\cdot n} =$$
$$\frac{e^{-2a(N+1)}(e^{-2a}+(N+1)-(N+1)e^{-2a})}{(1-e^{-2a})^2},$$

Therefore:

$$\lambda_m^{\omega}\cdot e^{-\eta(m+1)}\sqrt{\sum_{n=N+1}^{\infty}ne^{-2\eta n}} =$$
$$\lambda_m^{\omega}\cdot e^{\eta(m+1)}\frac{e^{-\eta(N+1)}\sqrt{e^{-2\eta}+(N+1)-(N+1)e^{-2\eta}}}{1-e^{-2\eta}}.$$

By choosing $m = N$:

$$\leq \lambda_N^{\omega}\cdot\frac{\sqrt{N+1}}{1-e^{-2\eta}}.$$

As a consequence:

$$\left|\sum_{n=N}^{\infty}\lambda_n^{\omega}a_n\cdot\sqrt{n+0.5}\right| \underset{\substack{Cauchy-Schwarz\\ inequality}}{\leq} \sqrt{\sum_{n=N}^{\infty}|a_n|^2}\cdot\lambda_N^{\omega}\cdot\frac{\sqrt{N+1}}{1-e^{-2\eta}}.$$

ACKNOWLEDGMENT

This research was supported in part by the Ollendorff Minerva Center. Minerva is funded through the BMBF.

REFERENCES

[1] D. Slepian and H. O. Pollak, "Prolate Spheroidal Wave Functions, Fourier Analysis and Uncertainty" Bell Systems Technical J 40, pp. 43-63, 1961.

[2] J. Knab "Interpolation of Band-Limited Functions Using the Approximate Prolate Series". IEEE Trans. on Information Theory Vol. IT–25, No 6, pp. 717-720, 1979.

[3] A. Osipov, "Non Asymptotic Analysis of Band-Limited Functions". Research report YALEU/DCS/TR-1449, 2012.

[4] D Slepian and E Sonnenblick, "Eigenvalues Associated with Prolate Spheroidal Wave Functions of Zero Order". Bell Systems Technical J 44, pp. 1745–1759, 1965.

[5] M Jeruchin, P Balaban and K Shanmugan, "Simulation of Communication Systems Modeling, Methodology and Techniques", 2nd Edition, Springer, 2000.

[6] H. Kirshner and M. Porat, "On the Approximation of L2 Inner Products from Sampled Data", IEEE Trans. on Signal Processing, Vol. 55, No. 5, pp. 2136-2144, 2007.

[7] T. G. Dvorkind, H. Kirshner, Y. C. Eldar and M. Porat, "Minimax Approximation of Representation Coefficients From Generalized Samples", IEEE Trans. on Signal Processing, Vol 55, No. 9, pp. 4430-4443, 2007.